Journal of Alloys and Compounds 509 (2011) 2304–2310

Contents lists available at ScienceDirect

Journal of Alloys and Compounds

journal homepage: www.elsevier.com/locate/jallcom

Effect of $BiAlO_3$ modification on the stability of antiferroelectric phase in $PbZrO_3$ ceramics prepared by conventional solid state reaction

Naratip Vittayakorn [a,b,c,*], Banjong Boonchom [d]

[a] College of KMITL Nanotechnology, King Mongkut's Institute of Technology Ladkrabang, Bangkok 10520, Thailand
[b] Department of Chemistry, Faculty of Science, King Mongkut's Technology Ladkrabang, Bangkok 10520, Thailand
[c] Thailand Center of Excellence in Physics (ThEP), CHE, 328 Si Ayutthaya Rd., Bangkok 10400, Thailand
[d] King Mongkut's Institute of Technology Ladkrabang, Chumphon Campus, 17/1 M.6 Pha Thiew District, Chumphon 86160, Thailand

ARTICLE INFO

Article history:
Received 7 September 2010
Received in revised form 28 October 2010
Accepted 28 October 2010
Available online 10 November 2010

Keywords:
Energy storage materials
Ferroelectrics
X-ray diffraction
Dielectric response

ABSTRACT

In this paper, we report on the polycrystalline $(Pb_{(1-3x/2)}Bi_x)(Zr_{1-3x/4}Al_x)O_3$ (PZO–BAO) ceramics, with $x = 0.0$–0.3, prepared by conventional solid state reaction. The crystal structure and thermal and dielectric properties of the sintered ceramics were investigated as a function of composition by means of X-ray diffraction (XRD), differential scanning calorimetry (DSC) and dielectric spectroscopy. The results indicated that the presence of $BiAlO_3$: BAO in the solid solution decreased the structural stability of the overall perovskite phase. Dielectric, thermal and P–E hysteresis results confirmed that no ferroelectric intermediate phase was seen in the PZO–BAO system. An antiferroelectric phase can be stable in a wide temperature range, indicating that BAO enhanced antiferroelectric phase stability in perovskite PZ manifests by "square" antiferroelectric behavior. Therefore, the $(Pb_{(1-3x/2)}Bi_x)(Zr_{1-3x/4}Al_x)O_3$ solid solution offers a material system for high-energy-storage capacitors and electromechanical transducers.

1. Introduction

Pure and compositionally modified lead zirconate ($PbZrO_3$; PZO) ceramics are important materials used in energy storage applications for DC fields, due its antiferroelectric (AFE) nature. PZO has an orthorhombic structure, with the lattice parameters, $a = 5.884$ Å, $b = 11.768$ Å and $c = 8.22$ Å [1]. The phase transition sequence has been found to follow the progressive heating of PZO orthorhombic AFE to rhombohedral ferroelectric (FE) ($228 < T < 230$ °C) to paraelectric (PE) cubic at $T_c = 230$ °C. The FE phase of between 228 and 230 °C is sometimes called the FE intermediate phase. The AFE-FE phase transition could occur spontaneously, due to several factors, for example, a change in stress configuration promoted by external mechanical driving fields, an increase in the amplitude of the applied AC electric field, hydrostatic pressure and/or temperature variations [2,3]. For electric field induced AFE to FE phases, transformation requires a very strong electric field in the AFE PZO, otherwise dielectric breakdown occurs instead. Therefore, most AFE ceramics are modified chemically by adding metal oxide at the A- and B-sites of the perovskite structure. The FE intermediate phase can be induced by adding Ba^{2+}, Sr^{2+}, and La^{3+} at the Pb^{2+}-site [2,4–7]. Moreover, our recent research found that the FE intermediate phase also can be induced by adding, for example, hybrid-doped Ni^{2+}/Nb^{5+}, Zn^{2+}/Nb^{5+}, Co^{2+}/Nb^{5+} and Mg^{2+}/W^{6+} at the Zr^{4+}-site [8–14].

$BiMO_3$; M = Fe^{3+}, Mn^{3+} and Nd^{3+} has received a lot of attention recently as a multiferroic, and investigation of the solid solutions, $BiMO_3$–$PbTiO_3$, has shown that they improve ferroelectric properties of $PbTiO_3$, reduce the amount of lead, and find new morphotropic phase boundary piezoelectrics [15–18]. However, very little has been known so far about experimental $BiMO_3$ with nonmagnetic ions (M = Al, Sc, Ga, and In). Furthermore, due to the relatively small size of Bi^{3+}, $Bi(M)O_3$ is not stable in perovskite form, and can be only synthesized under high pressure [19]. The smaller tolerance factor of $Bi(M)O_3$, and easily polarized Bi^{3+} ion, can enhance the transition temperature further, and with larger piezoelectric effect when solid solution with $PbTiO_3$ [15]. Crystallized $BiAlO_3$ is a noncentrosymmetric structure and isotypic with the well-known multiferroic, $BiFeO_3$. Theoretical studies by Baettig et al. [20], on a unique ferroelectric phase bismuth aluminate ($BiAlO_3$; BAO), predicted that BAO could be a promising novel candidate ferroelectric material, with a high curie temperature of ~530 °C. In 2005, Belik et al. [21] synthesized the compound of BAO by using a high-pressure, high-temperature technique at 6 GPa and 1000–1200 °C. BAO has rhombohedral (R3c) symmetry with lattice parameters given as $a = b = 5.37546(5)$ Å and $c = 13.3933(1)$ Å. Unfortunately, pure stable perovskite BAO ceramics have never been synthesized using a conventional sintering process, due to

* Corresponding author at: Department of Chemistry, Faculty of Science, King Mongkut's Institute of Technology Ladkrabang, Bangkok 10520, Thailand.
Fax: +66 2 326 4415.
E-mail address: naratipcmu@yahoo.com (N. Vittayakorn).

0925-8388/$ – see front matter © 2010 Elsevier B.V. All rights reserved.
doi:10.1016/j.jallcom.2010.10.206

the small value of t and electronegativity difference between A- and B-site cations. Zuo et al. [22] investigated the phase transitional behavior and various electrical properties of $(1-x)K_{1/2}Na_{1/2}NbO_3$; KNN–$x$BAO ceramics. The results indicate that the addition of BAO significantly influences the sintering, microstructure, phase transition and electrical properties of KNN ceramics. The identification of phase transitional behavior confirms the formation of a MPB between orthorhombic and tetragonal ferroelectric phases in the composition range of $0.005 \leq x \leq 0.01$. Ranjan et al. [23] studied the crystal structure and solid solubility in the $PbTiO_3$–$BiAlO_3$ system. Their study suggested that decrease in stability of the ferroelectric state, due to dilution of the Ti-sublattice by smaller sized Al^{3+} ions, was compensated for by the increase in ferroelectric stability by Bi^{3+} ions. Although the compositions of $Bi(M)O_3$–$PbTiO_3$ have been investigated widely, few reports on $Bi(M)O_3$ with other lead perovskite end members are available. To the authors' knowledge, the literature has not reported BAO as incorporated into PZO for solid solutions. Moreover, the effects of substitution in both A- and B-sites on the antiferroelectric phase stability of PZO are still unclear. The Bi^{3+} ion and Al^{3+} ion are both smaller than the Pb^{2+} and Zr^{4+} ion, respectively. Therefore, in this paper, we report on the how antiferroelectric phase stability is changed by A- and B-site substitution and determine the solubility limit of BAO in PZO.

2. Experimental procedures

2.1. Synthesis

Ceramics of $(Pb_{(1-3x/2)}Bi_x)(Zr_{1-3x/4}Al_x)O_3$, with $x = 0.0$–0.3, were synthesized using the conventional ceramic processing procedures [24]. Reagent grade oxide powders of Bi_2O_3 (≥99.9% purity, Cerac), PbO (≥99% purity, Kento), ZrO_2 (≥99.9% purity, Advance Material) and Al_2O_3 (≥99.5% purity, Fluka) were weighed according to stoichiometric formula, and ball-milled with ethanol and yttrium-stabilized zirconia media for 18 h. The dried powders were calcined in crucibles at 700–900 °C for 4 h, then ball-milled again for 6 h. The dried calcined powders were mixed with 5 wt% polyvinyl alcohol (PVA) and then pressed into pellets of 15 mm diameter and ~2 mm thickness. After burning out PVA binder at 550 °C, the pellets covered with extra powders were sintered in sealed crucibles at between 1100 °C and 1250 °C for 4 h.

2.2. Characterizations

The densities of ceramics were obtained using the Archimedes method. The density of the sintered PZO-BAO pellets was measured by the Archimedes water immersion method. The relative density of all the sintered pellets was approximately 97–98% of the theoretical density. X-ray diffraction (XRD; Bruker-AXS D8) using CuK_α radiation was utilized to determine the phases formed and optimum firing temperatures for formation of the desired phase for $0.02 \leq x \leq 0.3$ compositions. For measuring the dielectric and ferroelectric characteristics, the specimens were polished to 1 mm thickness using sand paper after ultrasonic cleaning in an ethanol bath. Silver-paste (Heraeus C1000) was coated on both sides of the sintered samples by the screen printing method, and then subsequently fired at 650 °C for 30 min. For investigating the dielectric properties, capacitance was measured at 1 kHz using an automated measurement system. This system consisted of an LCR meter (HP-4284, Hewlett-Packard Inc.). The dielectric constant was then calculated from $\varepsilon_r = Cd/\varepsilon_o A$, where C was the capacitance of the sample; d and A were the thickness and area of the electrode, respectively; and ε_o was the dielectric permittivity of vacuum (8.854×10^{-12} F/m). Polarizations, as a function of electric field (P–E loop) at 4 Hz of the samples, were observed using a ferroelectrics test system (RT66B; Radiant Technologies, Inc.). The peak field was maintained at 40 kV/cm during measurement.

3. Results and discussion

3.1. Crystal structure and physical properties of PZO–BAO solid solutions

The X-ray diffraction patterns of the sintered ceramics, $(Pb_{(1-3x/2)}Bi_x)(Zr_{1-3x/4}Al_x)O_3$; $x = 0.02$–0.3, at room temperature are shown in Fig. 1. The presence of diffraction peaks can be used to evaluate the structural order at long range or periodicity of the material [25]. The patterns indicate that the ceramics possess a phase of perovskite structure, and the crystalline symmetry is

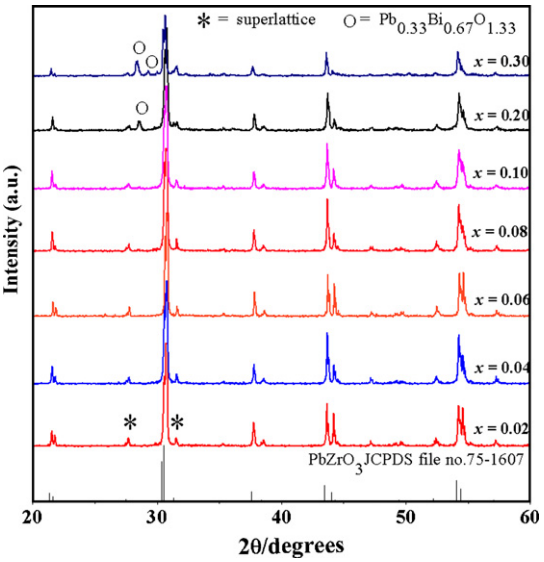

Fig. 1. XRD diffraction patterns of sintered $(Pb_{(1-3x/2)}Bi_x)(Zr_{1-3x/4}Al_x)O_3$; $x = 0.02$–0.30 ceramics.

orthorhombic. Phase-pure perovskite structures, with orthorhombic symmetry, were obtained for $x \leq 0.1$; however $x \geq 0.1$, A cubic pyrochlore phase $Pb_{0.33}Bi_{0.87}O_{1.33}$ (Powder diffraction Files no. 85-0448), identified by "o", began to develop at $x \geq 0.1$, and increased in intensity with increasing BAO concentration. These results indicated that the presence of BAO in the solid solution decreases the structural stability of PZO perovskite phase, due to the instability of BAO perovskite under normal conditions and the tolerance factor. The solubility limit of $(Pb_{(1-3x/2)}Bi_x)(Zr_{1-3x/4}Al_x)O_3$ ceramics is the composition, $x = 0.1$. The peak positions shifted to higher angles, indicating a slight decrease in the lattice parameter. This phenomenon can be explained qualitatively with respect to the unit cell volume caused by the Bi^{3+} and Al^{3+} incorporation. The ionic radii of Bi^{+3} (Shannon radius = 1.17 Å for CN = 8) and Al^{+3} (Shannon radius = 0.535 Å for CN = 6) are less than those of Pb^{+2} (Shannon radius = 1.29 Å for CN = 8) and Zr^{+4} (Shannon radius = 0.72 Å for CN = 6), respectively [26]. Therefore, Bi^{3+} can enter the eight-fold coordinated A-site of the perovskite structure to substitute Pb^{2+}, and Al^{3+} can enter the six-fold coordinated B-site of the perovskite structure to substitute Zr^{4+}, due to radius matching. The lattice parameters were calculated using the least square refinement from the UNITCELL-97 program [27]. Table 1 shows the lattice parameter and cell volume of $(Pb_{(1-3x/2)}Bi_x)(Zr_{1-3x/4}Al_x)O_3$ ceramics. The substitution of the relatively smaller Bi^{3+} and Al^{3+} for the comparatively larger Pb^{2+} and Zr^{4+} led to a decrease in the unit cell volume. This seems to be the case for $x \leq 0.01$ only, as composition, $x \geq 0.01$, is close to the solubility limit, but this argument does not apply due to the inhomogeneous distribution factor.

Fig. 2 shows enlarged profiles of the 1/4 (hkl) superlattice reflection (*) and (240)/(004) for determining the crystal structure of as-sintered ceramics. By increasing BAO concentration, the remaining 1/4 (hkl) superlattice reflection peaks indicated the remainder of antiparallel displacements of A-site ions in the perovskite structure. It is interesting to note that the substitution of BAO does not change the crystalline structure of PZO ceramics within the studied doping level. The influence of BAO addition on the phase structure of the PZO–BAO system is similar to that of the PT-BAO system [23,28]. The tolerance factor (t) for perovskite structure can be described by the general formula for ABO_3; $t = (R_A + R_O)/(\sqrt{2})(R_B + R_O)$, where R_A is the radius of A(CN = 8), R_B the radius of B(CN = 6) and R_O the radius of oxygen(CN = 8). When t is >1, the FE phase is stabilized, and when t is <1, the AFE phase is sta-

Table 1
Summary of the lattice parameters of $(Pb_{(1-3x/2)}Bi_x)(Zr_{1-3x/4}Al_x)O_3$; $x = 0.02$–0.1 ceramics.

Composition (x)	Lattice parameters			Volume of unit cell (Å^3)
	a	b	c	
0.00	5.8835 ± 0.0003	11.7672 ± 0.0008	8.2177 ± 0.0007	568.93
0.02	5.8629 ± 0.0207	11.7258 ± 0.0414	8.2171 ± 0.0273	564.89
0.04	5.8609 ± 0.0225	11.7221 ± 0.0453	8.2116 ± 0.0253	564.15
0.06	5.8584 ± 0.0237	11.7167 ± 0.0473	8.2023 ± 0.0195	563.01
0.08	5.8545 ± 0.0258	11.7113 ± 0.0494	8.2022 ± 0.0159	562.37
0.10	5.8522 ± 0.0275	11.7106 ± 0.0527	8.2007 ± 0.0124	562.01

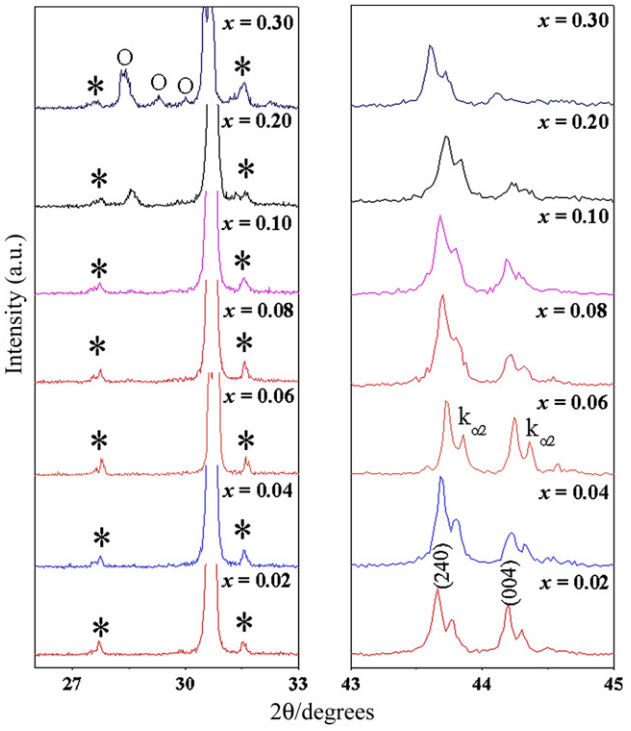

Fig. 2. X-ray diffraction profiles for the 1/4 (hkl) superlattice reflection (*), pyrochlore phase (○) and (240)/(004) peaks of $(Pb_{(1-3x/2)}Bi_x)(Zr_{1-3x/4}Al_x)O_3$; $x = 0.02$–0.30 ceramics.

bilized [29]. The average ionic radius of the A- and B-site ions in the $(Pb_{(1-3x/2)}Bi_x)(Zr_{1-3x/4}Al_x)O_3$ can be calculated from the following equation:

$$r_{\text{A-site}} = \left(1 - \frac{3x}{2}\right) r_{Pb^{2+}} + x r_{Bi^{3+}} \quad (1)$$

$$r_{\text{B-site}} = \left(1 - \frac{3x}{4}\right) r_{Zr^{4+}} + x r_{Al^{3+}} \quad (2)$$

where the ionic radii of Pb^{2+}, Bi^{3+}, Zr^{4+} and Al^{3+} are 1.29 Å, 1.17 Å, 0.72 Å and 0.535 Å, respectively [26]. The average ionic radius of the A- and B-site ions and tolerance factor in the $(Pb_{(1-3x/2)}Bi_x)(Zr_{1-3x/4}Al_x)O_3$ ceramics are shown in Table 2. The calculated tolerance factor of the $(Pb_{(1-3x/2)}Bi_x)(Zr_{1-3x/4}Al_x)O_3$; $x = 0.02$–0.3 is between 0.8904 and 0.8202, indicating that AFE behavior is expected to be seen at room temperature. Dielectric and ferroelectric properties; later explained, support this assumption. Furthermore, as expected, the stability of perovskite structure decreases with increasing BAO concentration, due to the small tolerance factor value.

3.2. Dielectric properties

Temperature dependence of relative permittivity (ε_r) and dielectric loss ($\tan\sigma$) for $(Pb_{(1-3x/2)}Bi_x)(Zr_{1-3x/4}Al_x)O_3$; $x = 0.02$–0.3 ceramics were measured at 1, 10 and 100 kHz, as shown in Fig. 3. It is well known that pure PZO has two dielectric anomaly peaks reported at 228 and 230 °C, which corresponds to the phase transitions of orthorhombic antiferroelectric (AFE) phase to rhombohedral FE intermediate phase and rhombohedral FE intermediate phase to cubic paraelectric phase, respectively. Furthermore, the FE intermediate phase can be induced easily by adding Ba^{2+}, Sr^{2+}, and Ca^{2+} at the Pb^{2+}-site [2,4–7] or Ni^{2+}/Nb^{5+}, Zn^{2+}/Nb^{5+}, Co^{2+}/Nb^{5+} and Mg^{2+}/W^{6+} at the Zr^{4+}-site [8–14]. As shown in Fig. 3, a single sharp dielectric permittivity peak arises in all ceramic samples. Interestingly, the dielectric results showed one sharp dielectric peak anomaly, indicating that the FE intermediate phase did not exist in $(Pb_{(1-3x/2)}Bi_x)(Zr_{1-3x/4}Al_x)O_3$; $x = 0.02$–0.3 samples. Increasing BAO concentration resulted in a very small decrease in transition temperature. No frequency dependence of dielectric response or shift in transition temperature with frequency was observed under transition temperature, which indicated no evidence of relaxor-like $Pb(Zr,Ni,Nb)O_3$ [8,10] or $(Pb,Ba)ZrO_3$ [5,7]. Nevertheless, at high temperature, the dielectric data revealed an enhanced dielectric loss with increasing BAO concentration. At 1 kHz measurement, frequent higher losses were found to persist to a significantly lower temperature. These results demonstrated that the enhanced dielectric losses at higher temperatures are due to a space charge mechanism [30]. For the composition, $x \geq 0.2$, the maximum relative permittivity decreases steadily with increasing BAO content (ε_r decreases from ~3700 in composition $x = 0.1$–700 in composition $x = 0.3$), and the lower value is attributed to the detrimental effect of the secondary pyrochlore phase.

Table 2
Average ionic radius of A-site, B-site ions and tolerance factor in the $(Pb_{(1-3x/2)}Bi_x)(Zr_{1-3x/4}Al_x)O_3$ ceramics.

Compositions (x)	$R_{\text{A-site}}$	$R_{\text{B-site}}$	Tolerance factor (t)
0.02	1.2747	0.7199	0.8904
0.04	1.2594	0.7198	0.8854
0.06	1.2441	0.7197	0.8804
0.08	1.2288	0.7196	0.8754
0.10	1.2135	0.7195	0.8704
0.20	1.1370	0.7190	0.8453
0.30	1.0605	0.7185	0.8202

3.3. Thermal properties

The DSC technique was used as the second tool to confirm the phase transition of PZO–BAO ceramics. Fig. 4 shows the temperature dependences of the heat flow (DSC curves) obtained when heating the $(Pb_{(1-3x/2)}Bi_x)(Zr_{1-3x/4}Al_x)O_3$; $x = 0.02$–0.3 samples at the rate of 10 K/min^{-1}. A single endothermic peak was observed for all compositions. The peaks shifted slightly to lower temperatures with increasing BAO concentrations. This transition temperature corresponds to the Curie temperature of the AFE to PE transformation. However, there is no significant difference in the temperature of AFE to PE phase transition in the composition, $x \geq 0.08$. This could be related to appearance of the pyrochlore phase. The DSC results

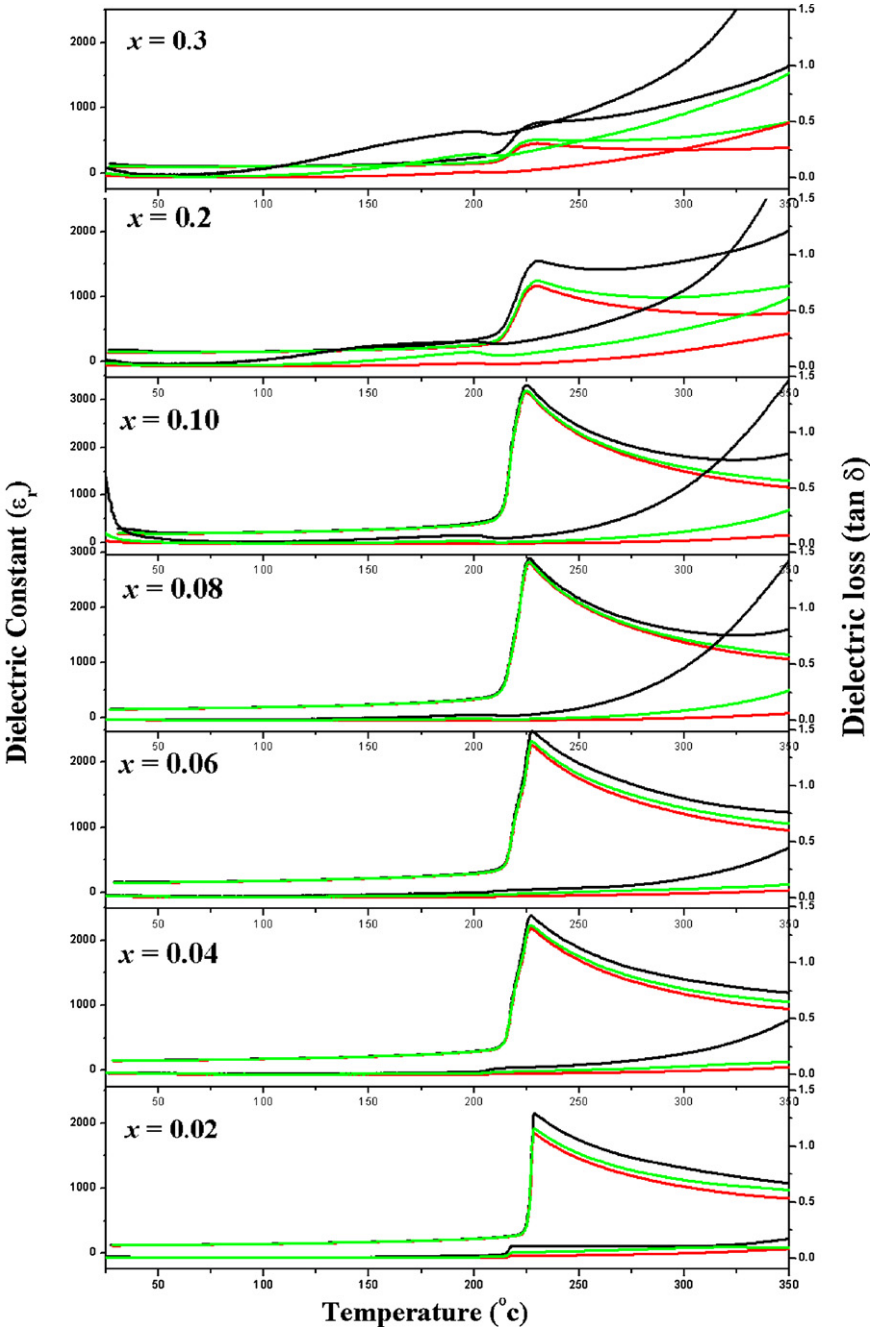

Fig. 3. Relative permittivity (ε_r) and dielectric loss ($\tan\delta$) as a temperature function of $(Pb_{(1-3x/2)}Bi_x)(Zr_{1-3x/4}Al_x)O_3$; $x = 0.02$–0.3 ceramics.

observed are consistent with dielectric measurement results. It should be pointed out that the difference in AFE-PE transition temperature values in dielectric, ferroelectric and DSC measurement techniques is due to the difference in heating rate and well time of the measurement.

Thermodynamic parameter, enthalpy ($\Delta H^*/J\,g^{-1}$), heat capacity ($C_p/J\,g^{-1}\,K^{-1}$), entropy change ($\Delta S^*/J\,g^{-1}\,K^{-1}$), and Gibbs energy change ($\Delta G^*/J\,g^{-1}$), were calculated from the DSC results. The enthalpy change was calculated directly from the amount of heat change involved in each step per unit mass of the sample. ΔH^*, thus determined, was implemented to calculate the specific heat capacity (C_p) using the following equation [31,32]

$$C_p = \frac{\Delta H}{\Delta T} \tag{3}$$

where $\Delta T = T_2 - T_1$; T_1 is the temperature at which the DSC peak begins to depart from the baseline; and T_2 is the temperature at which the peak lands. Consequently, the changes of entropy (ΔS^*) and Gibbs energy (ΔG^*) were calculated using the following equations [31,32]

$$\Delta S^* = 2.303 C_p \log\left(\frac{T_2}{T_1}\right) \tag{4}$$

$$\Delta H^* = \Delta G^* - T_p \Delta S^* \tag{5}$$

On the basis of the DSC data, the value of ΔH^*, ΔS^*, C_p and ΔG^* for the phase transition can be calculated according to Eqs. (3)–(5), and is presented in Table 3. The peak value of heat capacity became weaker, and anomaly of heat capacity gradually broader, with increasing BAO concentration. These results indicated that the phase transition deviates gradually from the first

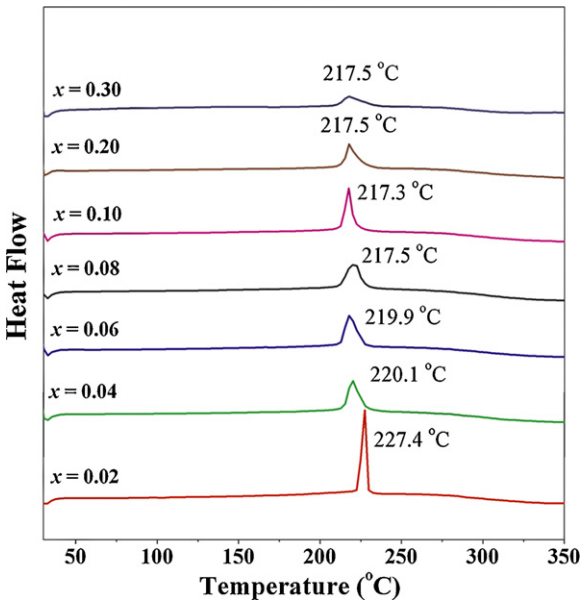

Fig. 4. Typical DSC curves for $(Pb_{(1-3x/2)}Bi_x)(Zr_{1-3x/4}Al_x)O_3$; $x = 0.02–0.3$ ceramics.

order type. Furthermore, the enthalpy (ΔH^*) continues to decrease with increasing BAO content, indicating that BAO decreases the energy requirement for transition from AFE to FE. Stenger and Burggraaf [33] observed that the change in entropy (ΔS^*) correlates with the fluctuation probability in conjunction with a small spontaneous lattice deformation and polarization. With increasing BAO content, there is no significant change in ΔS^*, indicating the stability of energy required to reorient the antiferroelectric sublattices in the PZO–BAO system [33]. On the other hand, the thermodynamic parameter, ΔH^* and ΔG^*, calculated according to Eqs. (3)–(5), gives the positive values, indicating that the AFE to PE phase transitions are connected to the introduction of heat, and phase transitions are non-spontaneous processes.

3.4. Ferroelectric properties

In order to examine how the phase transition occurs with temperature, electrical polarization hysteresis loop measurements were performed under a peak field of 40 kV/cm at a series of temperatures for $(Pb_{(1-3x/2)}Bi_x)(Zr_{1-3x/4}Al_x)O_3$ ceramics. A disk specimen, with a diameter of about 10 mm and thickness around 600 μm was used. The loop was recorded after the temperature was stabilized for at least 5 min. At 30 °C, no ferroelectric hysteresis loop was observed for any compositions ($0.0 \le x \le 0.3$). The linear polarization was observed, due perhaps to the extremely high coercive field, indicating that the composition, $x \le 0.3$, belongs to the AFE phase at room temperature. The $Pb_{0.94}Bi_{0.04}Zr_{0.97}Al_{0.04}O_3$ ceramic was selected for further investigation of the polarization behavior sequence during heating to 220 °C. The polarization behavior of $Pb_{0.94}Bi_{0.04}Zr_{0.97}Al_{0.04}O_3$ ceramic as a function of temperature is shown in Fig. 5. For the $Pb_{0.94}Bi_{0.04}Zr_{0.97}Al_{0.04}O_3$ composition, such linear behavior with minimum polarization remains at temperatures of up to 195 °C. When the temperature was raised to 200 °C, a double hysteresis loops started to develop, indicating the occurrence of electric field-induced antiferroelectric-to-ferroelectric phase transition. The transition from a minor loop at low field to a saturated double-shaped hysteresis loop at high field occurs at 205 °C by increasing the electric fields. This is expected because an antiferroelectric crystal generally has a zero net switchable dipole moment, due to the antiparallel alignment of elementary dipoles in its unit cell. When the external electric field is weak, the induced polarization is proportional to the electric field and demonstrates no macroscopic polarization hysteresis [34]. While the electric field exceeds a threshold value, called the critical field, the crystal becomes ferroelectric and the polarization displays hysteresis with respect to the field. A hysteresis loop also forms in the negative field, with the two loops being associated with antiparallel dipoles in adjacent unit-cell sublattices. As the temperature increases to 215 °C, the critical field is slowly reduced. This is caused by a higher temperature that provides higher thermal fluctuation to the polarization order parameter, which reduces the ferroelectric interaction among the dipoles.

In addition, when the temperature was increased to above 225 °C, a linear curve also was seen as an indication of the cubic paraelectric (PE) phase. Fig. 6 shows the polarization versus electric field hysteresis loops at 205 °C for the $(Pb_{(1-3x/2)}Bi_x)(Zr_{1-3x/4}Al_x)O_3$; $x = 0.02–0.08$ ceramics. The double hysteresis behavior in polarization, with an applied electric field, clearly demonstrates the antiferroelectric nature of $(Pb_{(1-3x/2)}Bi_x)(Zr_{1-3x/4}Al_x)O_3$; $x = 0.02–0.08$ ceramics. The remanent polarization, P_r, slightly decreases between $x = 0.02$ and 0.08, from 23.26 μC/cm^2 to 19.4 μC/cm^2. The AFE-FE switching field decreases for $x = 0.02$ and 0.08 from 29.23 kV/cm to13.81 kV/cm. In Berlincourt's [35] study of doped Pb(Zr,Sn,Ti)O_3 ceramics, two different types of AFE to FE transitions based on the character of the P–E hysteresis loop were described; the two types of double hysteresis loops have been termed "square" and "slanted". The "slanted" double hysteresis loop ceramics have far less hysteresis, small volume difference between AFE and FE phases, lower transition fields and a wider temperature range, over which the transition can be induced by electric fields. The "slanted" double hysteresis loop ceramics exhibit a small remanent polarization at zero fields, while the "square" loop ceramics do not. The P–E hysteresis loop measurements demonstrate that the ferroelectric properties of ceramics in the PZO–BAO system shift gradually from "square" to "slanted" antiferroelectric behavior, with increasing BAO concentrations. Interestingly, with increasing temperatures from room temperature to 250 °C, antiferroelectric to ferroelectric intermediate phase transition was not observed in any compositions, which indicated no ferroelectric intermediate phase in the PZO–BAO ceramics. Chu et al. [36] pointed out that the area enclosed by the decreasing field part of the polarization-electric field trace represented a stored electrical energy density. The ferroelectric results show that the PZO–BAO ceramics have large polarization at a high electric field and a large area between the polarization axis and curve. There are indications that this

Table 3
Values of thermodynamic parameters for phase transition of the $(Pb_{(1-3x/2)}Bi_x)(Zr_{1-3x/4}Al_x)O_3$ ceramics calculated from DSC data.

Compositions (x)	T_p/K	ΔH^*/J g^{-1}	C_p/J g^{-1} K^{-1}	ΔS^*/J g^{-1} K^{-1}	ΔG^*/J g^{-1}
0.02	499	3.825	7.665×10^{-3}	6.145×10^{-5}	3.856
0.04	497	3.749	7.543×10^{-3}	6.163×10^{-5}	3.795
0.06	491	3.348	6.819×10^{-3}	6.438×10^{-5}	3.382
0.08	490	2.815	5.745×10^{-3}	6.336×10^{-5}	2.849
0.10	489	2.676	5.461×10^{-3}	6.193×10^{-5}	2.901
0.20	490	2.360	4.816×10^{-3}	6.851×10^{-5}	2.408
0.30	489	1.429	2.922×10^{-3}	5.985×10^{-5}	1.455

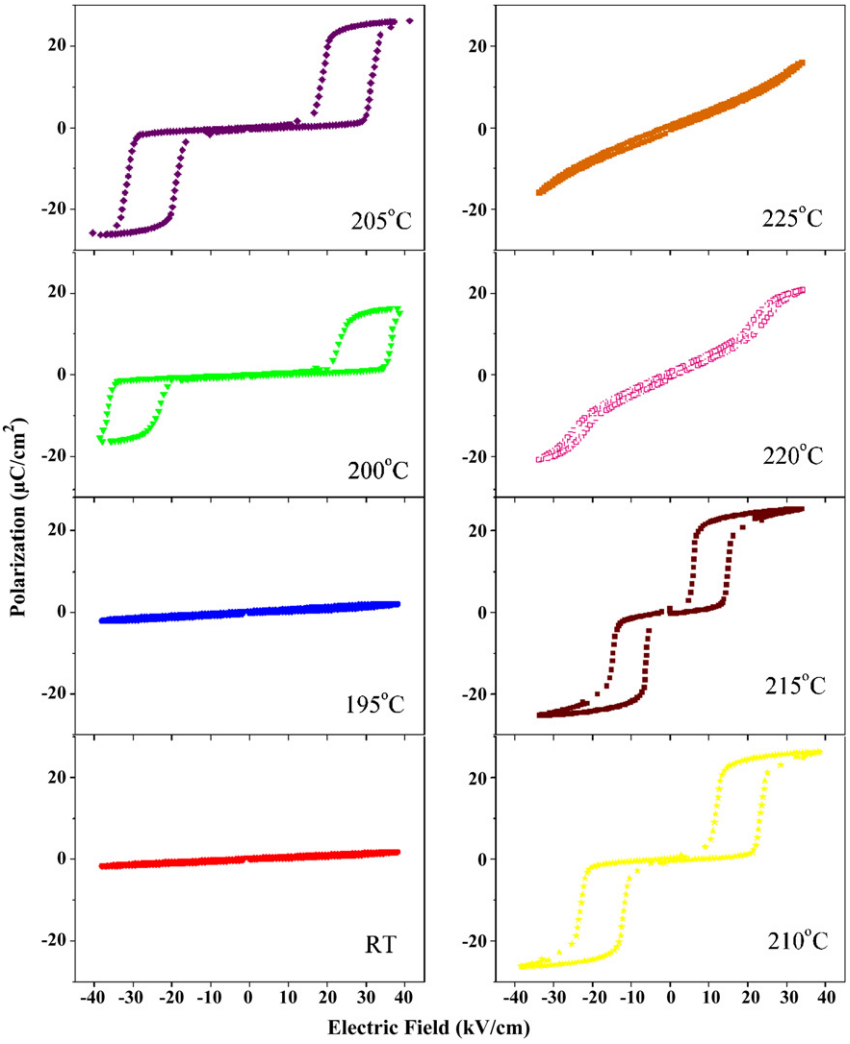

Fig. 5. Polarization hysteresis loops recorded from $Pb_{0.94}Bi_{0.04}Zr_{0.97}Al_{0.04}O_3$ ceramic at 4 Hz during heating.

material can therefore store much more energy than either the ferroelectric or linear dielectric materials.

There is good agreement between results of the three different investigation techniques. The results indicated that BAO modification can stabilize an antiferroelectric state in perovskite PZO. It is well known that the ionic size and distribution of substituent on the A- and B-site have been shown to affect antiferroelectric phase stability. If A-site ions are replaced by larger ones or a B-site ion by a smaller one, ferroelectric phase stability is enhanced. However, if A-site ions are replaced by smaller ones, or a B-site ion by a larger one, then antiferroelectric phase stability is enhanced [37]. However, in the PZO–BAO system, the ionic radius of Bi^{3+} (1.17 Å) and Al^{3+} (0.535 Å) are both smaller than Pb^{2+} (1.29 Å) and Zr^{4+} (0.72 Å), respectively. These results clearly demonstrate that the stability in antiferroelectric phase PZO, by substituting Pb^{2+} (1.29 Å) with Bi^{3+} (1.17 Å) in the A-site of the ABO_3 perovskite structure, are much more pronounced than substitution of Zr^{4+} by Al^{3+} in the B-site of the perovskite structure. This is because the decreasing average rate of radii in the A-site (0.765 Å/mol) is much higher than that in the B-site radii (0.005 Å/mol) as shown in Table 1. The decreasing average of radii in the A-site causes decreasing space in which the B-site cation is allowed to "rattle". This in turn decreases the polarizability, which facilitates a decrease in the Curie point. The results clearly demonstrated that the ionic radii of the substituent are an important factor in controlling the structure-property relations by compositional design.

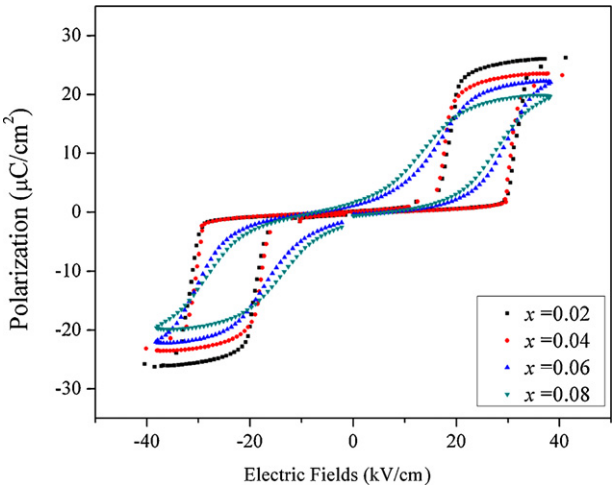

Fig. 6. Electric hysteresis loops of $(Pb_{(1-3x/2)}Bi_x)(Zr_{1-3x/4}Al_x)O_3$; $x = 0.02$–0.08 ceramics at 205 °C.

4. Conclusions

The investigation of $(Pb_{(1-3x/2)}Bi_x)(Zr_{1-3x/4}Al_x)O_3$; $x = 0.02$–0.3 using X-ray diffraction, dielectric behavior, thermal properties and ferroelectric measurements have shown clearly that phase

pure perovskite ceramics in the $(Pb_{(1-3x/2)}Bi_x)(Zr_{1-3x/4}Al_x)O_3$ system can be prepared by the solid-state reaction method with up to 10 mol% of $BiAlO_3$. Phase-pure perovskite structures with orthorhombic symmetry were obtained for $x \leq 0.1$; however $x \geq 0.1$, A cubic pyrochlore phase $Pb_{0.33}Bi_{0.87}O_{1.33}$ began to develop at $x \geq 0.1$ and increased in intensity with increasing BAO concentration. The substitution of the relatively smaller Bi^{3+} and Al^{3+} for the comparatively larger Pb^{2+} and Zr^{4+} led to a decrease in the unit cell volume. Dielectric, thermal and P–E hysteresis results confirmed that there was no ferroelectric intermediate phase in the PZO–BAO system, and only antiferroelectric to paraelectric phase transition was obtained for a wide temperature range. The results confirmed that BAO is shown to be a stable antiferroelectric state in PZO in a wide temperature range. The stability in antiferroelectric phase PZO by substituting Pb^{2+} (1.29 Å) with Bi^{3+} (1.17 Å) in the A-site of the ABO_3 perovskite structure is much more pronounced than substitution of Zr^{4+} by Al^{3+} in the B-site of the perovskite structure. The $(Pb_{(1-3x/2)}Bi_x)(Zr_{1-3x/4}Al_x)O_3$ solid solution offers a material system for possible applications in high-energy-storage capacitors and electromechanical transducers.

Acknowledgements

This research was supported by a grant from the Thailand Research Fund (TRF) National Research Council of Thailand (NRCT) and the National Nanotechnology Center (NANOTEC) NSTDA, Ministry of Science and Technology, Thailand, through its "Center of Excellence Network" program.

References

[1] F. Jona, G. Shirane, F. Mazzi, R. Pepinsky, Phys. Rev. 105 (1957) 849–856.
[2] D. Xunhu, Z. Xu, V. Dwight, J. Appl. Phys. 77 (1995) 5086–5094.
[3] X. Dai, J.F. Li, D. Viehland, Phy. Rev. B 51 (1995) 2651–2655.
[4] B.P. Pokharel, D. Pandey, J. Appl. Phys. 86 (1999) 3327–3332.
[5] B.P. Pokharel, D. Pandey, Phys. Rev. B 65 (2002) 214108.
[6] N. Vittayakorn, T. Bongkarn, G. Rujijanagul, Physica B 387 (2007) 415–420.
[7] X. Hao, Z. Zhang, J. Zhou, S. An, J. Zhai, J. Alloys Compd. 501 (2010) 358–361.
[8] S. Wirunchit, P. Laoratanakul, N. Vittayakorn, J. Phys. D: Appl. Phys. 41 (2008) 125406.
[9] N. Vittayakorn, S. Wirunchit, Smart Mater. Struct. 16 (2007) 851–857.
[10] S. Wirunchit, N. Vittayakorn, J. Appl. Phys. 104 (2008) 024103.
[11] W. Banlue, N. Vittayakorn, Ferroelectrics 382 (2009) 122–126.
[12] W. Banlue, N. Vittayakorn, Appl. Phys. A 93 (2008) 565–569.
[13] N. Vittayakorn, W. Banlue, Ferroelectrics 382 (2009) 110–114.
[14] P. Charoonsuk, S. Wirunchit, R. Muanghlua, S. Niemcharoen, B. Boonchom, N. Vittayakorn, J. Alloys Compd. 506 (1) (2010) 313–316.
[15] R.E. Eitel, C.A. Randall, T.R. Shrout, P.W. Rehrig, W. Hackenberger, S.E. Park, Jpn. J. Appl. Phys. 40 (2001) 5999–6002.
[16] C.J. Stringer, T.R. Shrout, C.A. Randall, I.M. Reaney, J. Appl. Phys. 99 (2006) 024106.
[17] M.R. Suchomel, P.K. Davies, J. Appl. Phys. 96 (2004) 4405–4410.
[18] M.R. Suchomel, P.K. Davies, Appl. Phys. Lett. 86 (2005) 262905.
[19] M.R. Suchomel, A.M. Fogg, M. Allix, H. Niu, J.B. Claridge, M.J. Rosseinsky, Chem. Mater. 18 (2006) 4987–4989.
[20] P. Baettig, C.F. Schelle, R. LeSar, U.V. Waghmare, N.A. Spaldin, Chem. Mater. 17 (2005) 1376–1380.
[21] A.A. Belik, T. Wuernisha, T. Kamiyama, K. Mori, M. Maie, T. Nagai, Y. Matsui, E. Takayama-Muromachi, Chem. Mater. 18 (2005) 133–139.
[22] R. Zuo, D. Lv, J. Fu, Y. Liu, L. Li, J. Alloys Compd. 476 (2009) 836–839.
[23] R. Ranjan, A.K. Kalyani, R. Garg, P.S.R. Krishna, Solid State Commun. 149 (2009) 2098–2101.
[24] T. Badapanda, S.K. Rout, L.S. Cavalcante, J.C. Sczancoski, S. Panigrahi, T.P. Sinha, E. Longo, Mater. Chem. Phys. 121 (2010) 147–153.
[25] L.S. Cavalcante, V.S. Marques, J.C. Sczancoski, M.T. Escote, M.R. Joya, J.A. Varela, M.R.M.C. Santos, P.S. Pizani, E. Longo, Chem. Eng. J. 143 (2008) 299–307.
[26] R.D. Shannon, Acta Cryst. A 32 (1976) 751–767.
[27] T.J.B. Holland, S.A.T. Redfern, Miner. Mag. 61 (1997) 65–77.
[28] A.K. Kalyani, R. Garg, R. Ranjan, Appl. Phys. Lett. 94 (2009) 202903.
[29] K.J. Rao, C.N.R. Rao, Phase Transitions in Solid: An Approach to the Study of the Chemistry and Physics of Solids, McGraw-Hill, New York, 1978.
[30] M.E. Lines, A.M. Glass, Principles and Applications of Ferroelectrics and Related Materials, Clarendon press, Oxford, 1977.
[31] S.A. Halawy, N.E. Fouad, M.A. Mohamed, M.I. Zaki, J. Therm. Anal. Calorim. 82 (2005) 671–675.
[32] R.H. Abu-Eittah, N.G. ZaKi, M.M.A. Mohamed, L.T. Kamel, J. Anal. Appl. Pyrol. 77 (2006) 1–11.
[33] C. Stenger, A.J. Burggraaf, Phys. Stat. Sol. 61 (1980) 275–285.
[34] F. Moura, A.Z. Simões, L.S. Cavalcante, M.A. Zaghete, J.A. Varela, E. Longo, J. Alloys Compd. 466 (1–2) (2008) L15–L18.
[35] D. Berlincourt, IEEE Trans. Sonics Ultrason. Ind. Eng. Chem. SU-13 (1966) 116–124.
[36] B. Chu, X. Zhou, K. Ren, B. Neese, M. Lin, Q. Wang, F. Bauer, Q.M. Zhang, Science 313 (2006) 334–336.
[37] Q. Tan, Z. Xu, D. Viehland, J. Mater. Res. 14 (1999) 4251.